Chin. Phys. Lett. **39**, 067501 (2022)

Microscopic Magnetic Origin of Rhombohedral Distortion in NiO

Guangmeng He(何光萌)[1,2†], Huimin Zhang(张慧敏)[1,2†], Jinyang Ni(倪斤阳)[1,2], Boyu Liu(刘博宇)[1,2], Changsong Xu(徐长松)[1,2*], and Hongjun Xiang(向红军)[1,2*]

[1]*Key Laboratory of Computational Physical Sciences (Ministry of Education), Institute of Computational Physical Sciences, and Department of Physics, Fudan University, Shanghai 200433, China*
[2]*Shanghai Qi Zhi Institute, Shanghai 200030, China*

(Received 21 March 2022; accepted 22 April 2022; published online 29 May 2022)

Numerous investigations have been conducted to explore the structural phase transition in antiferromagnetic $3d$ transition metal monoxides accompanied by appearance of magnetic phase transition. However, how the spins induce distortion in the high symmetric structure has not yet been fully understood. In this study, the monoxide NiO is used as an example to investigate what lowers the structural symmetry. By comparing two different magnetic structures, our results reveal that the spin–lattice coupling is responsible for such a structural distortion. Then, a spin–lattice model, including the strain component, is constructed to simulate the transition procedure. Moreover, the results from the first-principles calculations are used to compare with our model results. Both first-principles calculations and model simulations clarify the structural phase transition caused by a unique magnetic arrangement.

DOI: 10.1088/0256-307X/39/6/067501

Antiferromagnetic (AFM) Mott insulators not only are fundamentally crucial, but also have technical applications.[1–3] Among such Mott antiferromagnets, NiO is critical in studying electronic, magnetic, and structural properties of strong correlated $3d$ electron materials. In NiO, the partially occupied Ni d shell and strong superexchange interactions result in a high magnetic transition temperature ($T_{\rm N} = 523\,{\rm K}$),[4–6] making NiO a promising candidate for room-temperature spintronics applications.[7–9] Above $T_{\rm N}$, NiO crystallizes into the face-centered-cubic structure (space group $Fm\bar{3}m$) [Fig. 1(a)] in the paramagnetic state.[10] As the temperature decreases, a slight trigonal structural distortion appears and NiO crystallizes into the rhombohedral structure (space group $R\bar{3}m$) accompanying the existence of the AFM phase.[10–12] Such a distortion also happens in other antiferromagnets, such as MnO,[13–15] which may also have the same mechanism.

The AFM properties of NiO have been reported in the literature,[2] and its ground magnetic state is discovered to be a ferromagnetic (FM) (111) layer stacked antiferromagnetically along the [111] direction [Fig. 1(b)]. The [111] direction is set as the z axis in this study. The magnetic and structural phase transitions occur simultaneously due to the competition of nearest-neighbor (NN) and next-nearest-neighbor (NNN) exchange interactions.[16] The crystal structure contracts along the [111] direction from a cubic structure to a rhombohedral structure as the specific AFM arrangement emerges in NiO. The x-ray diffraction study by Rooksby and Slack showed that such a distortion causes the rhombohedral angle α [Fig. 1(a)] from 60° at high temperature to be 60.07° below the Neel temperature.[5] The distance of NNN Ni ions was measured to be 4.176 Å at 298 K and 4.171 Å near 0 K.[10]

Several attempts have been made to investigate the transition mechanism based on the structural distortion that accompanies the magnetic phase transition. Greenwald and Smart first proposed that the ordering of an antiferromagnet was responsible for the observed lattice distortions. They also highlighted that such distortion was induced by the exchange striction.[1] However, Li[17] proposed that NiO must have the type-B arrangement, as shown in Fig. 2(d), and considered that the distortion was induced by anisotropy magnetostriction. However, Roth[2] reported that magnetic dipole–dipole interactions predominated and type-A arrangement [Fig. 2(c)] should be the magnetic ground state. Further, Rodbell and Owen[15] derived an expression for the distortion with a molecular-field approach and proposed that the anisotropic strain plays a significant role in NiO and MnO. Other efforts have also been made to focus on the individual aspects of the structural distortions, such as single-ion magnetostriction,[18] Heisenberg model with distance-dependent interactions,[19] lattice dynamical property calculations,[20] and Heisenberg exchange analysis.[21] However, the relationship between the magnetic and structural phase transitions remains unclear and requires a more detailed study for interpretation.

†Guangmeng He and Huimin Zhang contributed equally to this work.
*Corresponding authors. Email: csxu@fudan.edu.cn; hxiang@fudan.edu.cn
© 2022 Chinese Physical Society and IOP Publishing Ltd

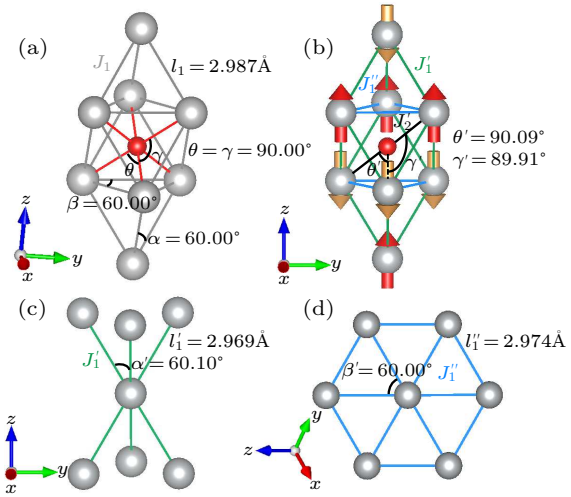

Fig. 1. (a)–(d) Grey sphere: Ni; red sphere: O. The red and yellow arrows represent the spin-up and spin-down states of Ni ions. Here, α, β, α', and β' denote the Ni–Ni–Ni angles, whereas γ, θ, γ', and θ' denote the Ni–O–Ni angles. The bond lengths are labeled l_1, l_1', and l_1''. (a) The relaxed structure in cubic symmetry, where J_1 and J_2 represent NN and NNN, respectively, exchange interactions. (b) The distorted crystal structure is optimized from the cubic structure with experimental parameters in case (iii). J_1 in high symmetry structure turns into different groups, J_1' and J_1'', due to the distortion. The bonds corresponding to J_1' and J_1'' are shown as green and blue lines, respectively. (c) J_1' represents the six-fold inter-plane exchange interactions. (d) J_1'' represents the six-fold intra-plane exchange interactions.

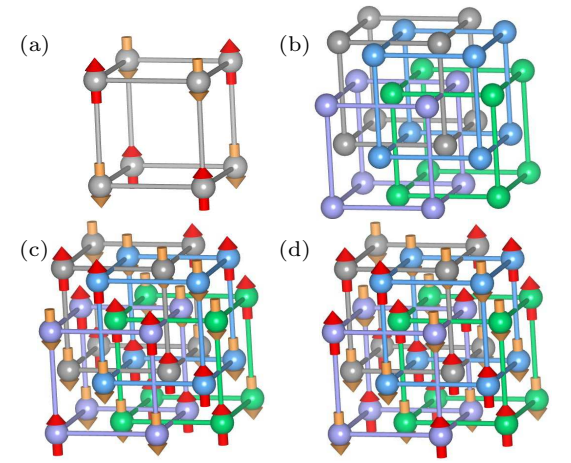

Fig. 2. (a) The simple-cubic sublattice in which two adjacent Ni ions are AFM. (b) The combination of the four sublattices marked in different colors. Each sublattice satisfies the AFM relationship shown in (a). (c) The type-A magnetic structure. (d) The type-B magnetic structure. The red arrows in (c) and (d) represent up-spins, and the yellow arrows represent down-spins. Note that only Ni ions are shown in spheres with green, blue, purple, and grey.

Both density functional theory (DFT) calculations and spin Hamiltonian model simulations were performed in this study. An effective spin Hamiltonian model is constructed to describe the energy of NiO within a cubic structure. Monte Carlo (MC) simulations with such Hamiltonian are performed to determine the magnetic ground states, i.e., types A and B. Further, symmetry analyses are performed to deduce that only type A with rhombohedral distortion is the magnetic and structural ground state. Notably, a spin–lattice model is proposed to analyze the microscopic mechanism of NiO's rhombohedral distortion. Meanwhile, the DFT calculations were performed as a means of comparison to verify the accuracy of our model study.

The DFT calculations are performed using the Vienna *ab initio* simulation package (VASP)[22,23] with the projector-augmented wave method. The Perdew–Burke–Ernzerhof functional is used to describe electron interactions,[24] and the generalized gradient approximation with Hubbard U (GGA+U) method is used to treat electron exchange and correlation. The Hubbard effective U is imposed on the $3d$ orbitals of the Ni ion using the Dudarev approach.[25] According to the previous studies,[3,26] U_{eff} ($U_{\text{eff}} = U - J$) is set to be 4.5 eV in our calculations. In addition, different U_{eff} values ranging from 4 to 6 eV are tested, and we found that a reasonable U_{eff} choice does not change our main results. The cut-off energy is 550 eV and Ni $3d$, O $2s$, and O $2p$ are considered to be valence states. The internal degrees of freedom are optimized by relaxation of shape of the unit cell and the atomic positions until the Hellmann–Feynman force is less than 1 meV/Å. For NiO, the unit cell contains one Ni ion and one O ion. A $2 \times 2 \times 2$ supercell is adopted to calculate the energies of different spin configurations, and the k-mesh is set to be $13 \times 13 \times 13$ for optimization and $19 \times 19 \times 19$ for static calculation. A $3 \times 3 \times 3$ supercell is constructed to calculate the parameters of magnetic interaction, with a k-mesh of $5 \times 5 \times 5$. The four-state method is used to calculate the quadratic exchange interaction parameters in this study,[27] using the formula

$$J_{ij} = \frac{E_{\uparrow\uparrow} + E_{\downarrow\downarrow} - E_{\uparrow\downarrow} - E_{\downarrow\uparrow}}{4S^2}, \tag{1}$$

where E_{gh} ($g, h = \uparrow, \downarrow$) represents the energies of different spin configurations, in which the sites i and j can change the spin direction. The other spins are set being perpendicular to that of sites i and j, and they remain unchanged during the calculation. The parameters of biquadratic exchange interactions, K_{ij}, can be obtained similarly by mapping the spins of sites i and j.[27] In addition, the coefficient $\partial J_{ij}/\partial \eta_p$ can be achieved using the four-state method[28] with the following formula:

$$\begin{aligned}\frac{\partial J_{ij}}{\partial \eta_p} &= \frac{1}{4}\left(\frac{\partial E_{\uparrow\uparrow}}{\partial \eta_p} + \frac{\partial E_{\downarrow\downarrow}}{\partial \eta_p} - \frac{\partial E_{\uparrow\downarrow}}{\partial \eta_p} - \frac{\partial E_{\downarrow\uparrow}}{\partial \eta_p}\right) \\ &= -\frac{1}{4}(\sigma_p^{\uparrow\uparrow} + \sigma_p^{\downarrow\downarrow} - \sigma_p^{\uparrow\downarrow} - \sigma_p^{\downarrow\uparrow}),\end{aligned} \tag{2}$$

where η_p ($p = 1, \ldots, 6$) is the homogeneous strain in Voigt notation and σ_p denotes the corresponding stress.

To describe the magnetic energy of undistorted cubic NiO, we adopt the effective spin Hamiltonian model expressed as

$$E(\boldsymbol{S}) = \sum_{i,j>i} J_1 \boldsymbol{S}_i \cdot \boldsymbol{S}_j + \sum_{l,k>l} J_2 \boldsymbol{S}_l \cdot \boldsymbol{S}_k + \sum_{i,j>i} K_1 (\boldsymbol{S}_i \cdot \boldsymbol{S}_j)^2 + \sum_{l,k>l} K_2 (\boldsymbol{S}_l \cdot \boldsymbol{S}_k)^2, \quad (3)$$

where J_1 and J_2 are the NN and NNN Heisenberg exchange interaction parameters, respectively; K_1 and K_2 are the NN and NNN biquadratic interactions, respectively. The biquadratic term is considered here because it is previously highlighted to be important for the d^8 configuration.[29] The spin value $\boldsymbol{S} = 1$ is adopted.

Table 1. The magnetic parameters of NiO at different symmetries. The values in parenthesis are measured experimentally in previous works. The unit is meV.

Cubic	Rhombohedral
$J_1 = -1.34$ (-1.37, Ref. [30])	$J_1' = -1.35$ (-1.36, Ref. [30]) $J_1'' = -1.38$ (-1.39, Ref. [30])
$J_2 = 22.29$ (17, 19.8, Refs. [30,31])	$J_2' = 23.22$
$K_1 = -0.13$	$K_1' = -0.13$ $K_1'' = -0.14$
$K_2 = -0.60$	$K_2' = -0.60$

The aforementioned exchange interaction parameters can be obtained from the DFT calculations with a relaxed structure in cubic symmetry[10] using the four-state energy mapping method, and our results are listed in Table 1. For the relaxed cubic structure [Fig. 1(a)], the NN superexchange interactions (J_1) are 12-fold degenerate with Ni–Ni coupled through a 90° Ni^{2+}–O^{2-}–Ni^{2+} path. The Ni–Ni–Ni angles marked as α and β are both 60°. The bond length of all NN Ni sites, l_1, is 2.987 Å within the cubic structure. J_1 is calculated to be -1.34 meV, implying the FM interactions due to the negative sign. However, the NNN superexchange interactions (J_2) are six-fold degenerate with Ni–Ni coupling through a 180° Ni^{2+}–O^{2-}–Ni^{2+} path. J_2 is simulated to be 22.29 meV, indicating AFM couplings. Our results for J_1 and J_2 are consistent with Goodenough's rule.[32] The FM nature of J_1 and the AFM of J_2 indicate exchange competition among NNs and NNNs. Notably, the derived J_1 and J_2 in our calculations are comparable with those of previous studies, as presented in Table 1, which proves the accuracy of our results. Moreover, the biquadratic parameters are also determined by the four-state method, yielding $K_1 = -0.13$ meV and $K_2 = -0.60$ meV, indicating the non-negligible fourth-order interactions. The negative biquadratic parameter favors collinear alignment, either parallel or antiparallel.

Further, MC simulations with such Hamiltonian are performed using differently sized and shaped supercells in $Fm\bar{3}m$ symmetry. The ground state is determined to be an AFM pattern [Fig. 2(c)]. Such a pattern is consistent with the reported configuration[17,33] and named type-A structure. Besides type-A, type-B is another low-energy (or degenerate) state that satisfies the NNN AFM relationship [Fig. 2(d)]. Note that type-A and type-B states are ordered states and have a similar contribution to the configurational entropy. Types A and B can be considered as the different coupling of four simple-cubic sublattices, with each sublattice satisfying a 180° Ni^{2+}–O^{2-}–Ni^{2+} AFM relationship. Figure 2(a) shows the simple-cubic sublattice. Figure 2(b) shows the combination of the four sublattices. Any two NN Ni ions are in different sublattices. In type A, the (111) planes are in the FM state, whereas two adjacent planes are in the AFM state, i.e., the magnetic ground state. However, the special spin arrangement is absent in type B. The DFT energies of types A and B in the cell, compared with MC simulations, yield a negligible difference of 0.001 meV/Ni, confirming our model simulation results. Further analyses show that each type-A or type-B configuration satisfies six pairs of the 12-fold FM NN interactions, six pairs of the 12-fold AFM NN interactions, and six pairs of the six-fold AFM NNN couplings. This suggests that type-A and B configurations would have the same energy if the effective spin Hamiltonian model shown in Eq. (3) is adopted. Such analyses explain the fact that types A and B are close in energy.

Table 2. The DFT energies of type-A and type-B structures under different optimization conditions. Note that E (iii) of type-A is set to be an energy reference.

Case	Type	E (meV/Ni)	The change of group symmetry
(i) Lattice vectors are frozen while atoms relaxed	A	8.51	Maintain $Fm\bar{3}m$
	B	8.51	Maintain $Fm\bar{3}m$
(ii) Lattice vectors are relaxed while atoms frozen	A	0	Transform to $R\bar{3}m$
	B	0.08	Maintain $Fm\bar{3}m$
(iii) Lattice vectors and atoms are both relaxed	A	0	Transform to $R\bar{3}m$
	B	0.08	Maintain $Fm\bar{3}m$

Now, we investigate why the type-A structure widely exists in nature, whereas type-B does not. Symmetry analyses are further performed considering types A and B when the optimization is applied. Three different approaches are used to optimize the cubic structure with experimental parameters using DFT calculations: (i) Lattice vectors are frozen while atoms are allowed to relax. (ii) Atoms are frozen while

lattice vectors are allowed to change. (iii) Atoms and lattice vectors are both relaxed. Table 2 summarizes the results of types A and B in different optimization methods. In case (i), types A and B have the same energy and both maintain the cubic symmetry due to the frozen lattice vectors. We discover that cases (ii) and (iii) produce the same results. For type A, the DFT structural optimization results in a distorted rhombohedral $R\bar{3}m$ structure, whereas type B maintains the cubic $Fm\bar{3}m$. Therefore, lattice distortion, rather than relative atomic displacements, causes rhombohedral distortion. The energy of type A with a distorted structure is 0.08 meV/Ni lower than that of type B in an undistorted structure, indicating that the distorted structure is the ground state structure.

Regarding the structural distortions, the NN interactions also lower their degeneracy. The distorted structure [Fig. 1(b)] is optimized from the cubic structure using experimental parameters in case (iii) and used to calculate the exchange interaction parameters. The NN pairs are divided into two groups, with $J_1' = -1.35$ meV being inter-(111) plane interactions and $J_1'' = -1.38$ meV being intra-(111) layer couplings. Figures 1(c) and 1(d) show the six-fold NN inter-plane J_1' and six-fold NN intra-plane J_1'', with the Ni–Ni–Ni angles, α' and β', and Ni–Ni bond lengths, l_1' and l_1''. Let us analyze the split of J_1 based on the changes of α, β, and l_1. The changes in angle and bond indicate a contraction along [111] direction. We can also conclude the structural contraction along the z-axis from the changes in the superexchange angle of Ni^{2+}–O^{2-}–Ni^{2+}. The angle of Ni^{2+}–O^{2-}–Ni^{2+} with Ni ions in adjacent (111) planes changes from 90° (γ) to 89.91° (γ') when an angle with Ni ions in the same (111) plane changes from 90° (θ) to 90.09° (θ'), which implies this contraction. Table 1 summarizes the parameters in a distorted structure due to the contraction, showing the previous results for comparison. Similar results from other studies confirm the accuracy of our calculation. Accordingly, the biquadratic interaction, K_1, also split into $K_1' = -0.13$ meV and $K_1'' = -0.14$ meV. In contrast, the NNN interaction maintains its degeneracy since all NNN interactions are inter-(111)-typed.

The rhombohedral distortion associated with the type-A configuration can be understood as follows. In the type-A configuration, the neighboring spins between the (111) layers are antiparallel to each other, whereas neighboring spins within each (111) layer are parallel to each other. To lower the spin interaction energy of the type-A configuration, the interlayer NN FM-exchange interaction should be weaker than the intralayer NN FM-exchange interaction. This is achieved in the rhombohedral structure with interlayer $J_1' = -1.35$ meV and intralayer $J_1'' = -1.38$ meV. The NiO lattice being contracted rather than elongated along the [111] direction is consistent with the modulation of the NN FM-exchange interactions. Two competing spin-exchange mechanisms exist for the NN exchange interaction with the 90° Ni–O–Ni angle: the AFM direct Ni–Ni exchange and the FM superexchange through the bridging of O-ion. By comparing interlayer and intralayer exchange interactions in the rhombohedral structure, the FM superexchange can be regarded as the same since the magnitude ($\propto |\cos(\angle\text{Ni–O–Ni})|$) of the effective $e_g - t_{2g}$ hopping is the same (note that $\theta' = 180° - \gamma'$). The AFM direct Ni–Ni exchange for the interlayer J_1' is stronger than that of the intralayer J_1'' as the interlayer Ni–Ni bond distance is shorter than that of the intralayer bond.

Table 3. The symmetrized elastic moduli C_{pq} of NiO obtained from cubic structure (kbar). The coordinate system is the same as that in Fig. 1.

	xx	yy	zz	xy	yz	zx
xx	3169	1247	1344	0	0	−138
yy	1247	3169	1344	0	0	138
zz	1344	1344	3071	0	0	0
xy	0	0	0	961	138	0
yz	0	0	0	138	1059	0
zx	−138	138	0	0	0	1059

Table 4. The magnetic parameters of the cubic structure of NiO. The coordinate system is the same as that in Fig. 1.

	xx	yy	zz	xy	yz	zx
$\frac{\partial J_1}{\partial \eta_p}$ (eV)	−0.004	0.008	−0.008	0	0	−0.004
$\frac{\partial J_2}{\partial \eta_p}$ (eV)	−0.049	−0.063	−0.055	−0.012	−0.017	−0.010

We now establish an effective model to further understand the microscopic mechanism of the rhombohedral distortion. Based on the preceding discussions, it is reasonable to consider elastic energy and spin–lattice couplings (rather than spin–phonon interactions) in such a model,[34] resulting in the following expressions:

$$E(\eta_p, \boldsymbol{S}) = E(\boldsymbol{S}) + \sum_{p,q} \frac{1}{2} C_{pq} \eta_p \eta_q V_0 + \sum_{i,j} \Big(\frac{\partial J_{ij}}{\partial \eta_p} \boldsymbol{S}_i \cdot \boldsymbol{S}_j \Big) \eta_p, \tag{4}$$

where the first part $E(\boldsymbol{S})$ is defined in Eq. (3), and the second part represents the elastic energy, with C_{pq} being the elastic moduli and η_p ($p = 1, \ldots, 6$) being the homogeneous strain in Voigt notion. The third part denotes the Taylor expansion of spin–lattice couplings concerning η_p, and only the NN and NNN Heisenberg exchange interactions are considered. The spin value of $|\boldsymbol{S}|$ is also set to 1. The relaxed structure in cubic symmetry is applied to obtain C_{pq} and $\partial J_{ij}/\partial \eta_p$ in DFT calculations and to perform the model simulations [Fig. 1(a)], and has a volume V_0. C_{pq} is given in Table 3, and the coefficients $\partial J_{ij}/\partial \eta_p$ are presented

in Table 4, which are calculated using Eq. (2), indicating how the strain affects the exchange parameters of the ordered NN pair [close to label l_1 in Fig. 1(a)] and NNN pair [shown in black solid line in Fig. 1(a)]. Any NN or NNN pair can be used for calculation due to the degenerate relationship in the cubic symmetry. Note that the coordinate system shown in Fig. 1 is applied here.

Table 5. The strain tensor induced by spin order in types A and B. The coordinate system is the same as that in Fig. 1.

Strain by spin order	xx	yy	zz	xy	yz	zx
Type A	−0.00173	−0.00173	−0.00391	0	0	0
Type B	−0.00246	−0.00246	−0.00246	0	0	0

We estimate the lattice distortion using the spin–lattice model and compare it with DFT calculations. The different magnetic structures, types A and B, in the cubic phase are both considered in the model. The strain η_p is the only variable in the model. We minimize the total energy $E(\eta_p, \boldsymbol{S})$ concerning η_p to obtain the structural distortion by spin order. Table 5 shows the strain tensor. For types A and B, the tensor only has nonzero diagonal elements, indicating that the strain merely occurs in the x, y, and z directions. For type A, the negative sign of the diagonal element indicates a shortened strain in a certain direction, and the absolute value of the z component is almost twice the value of the x or y component. Thus, a contraction along the z direction, i.e., the [111] direction, occurs and lowers the cubic symmetry. The diagonal elements for type B are the same, shrinking the overall volume but maintaining the cubic symmetry. Table 6 shows the structure parameters and symmetry at the beginning and final states, with the strain obtained from the spin–lattice model. The results of the aforementioned DFT calculations are also presented for comparison. For type A, the model results show that the structural ground state is $R\bar{3}m$, and the angle α (60°) changes to α' (60.097°), which is extremely close to the 60.100° obtained from DFT calculations. The bond length l is split into l' and l'' in both the methods. The changes in angle and bond length indicate a contraction along [111] direction. For type B, the structural ground state is $Fm\bar{3}m$, while α maintains 60° and l does not change into two groups in the final state from the model, which is consistent with the DFT calculations. Similar results from DFT calculations confirm the accuracy of the spin–lattice model.

Table 6. The Ni–Ni–Ni angle, α, and bond length l of NN Ni ions, and symmetry at the beginning and final states obtained from both the spin–lattice model simulations and DFT calculations for types A and B.

Type	Parameters	Model results		DFT calculations	
		Begin state	Final state	Begin state	Final state
A	α	60.000°	60.097°	60.000°	60.100°
	l	2.987 Å	2.977 Å 2.982 Å	2.953 Å	2.969 Å 2.974 Å
	Symmetry	$Fm\bar{3}m$	$R\bar{3}m$	$Fm\bar{3}m$	$R\bar{3}m$
B	α	60.000°	60.000°	60.000°	60.000°
	l	2.987 Å	2.980 Å	2.953 Å	2.971 Å
	Symmetry	$Fm\bar{3}m$	$Fm\bar{3}m$	$Fm\bar{3}m$	$Fm\bar{3}m$

To further examine whether it is $\partial J_1/\partial \eta_p$ or $\partial J_2/\partial \eta_p$ that causes the contraction along the [111] direction, we arbitrarily turn on and off each of the two terms in the spin–lattice model of Eq. (4). When starting with type A, it is discovered that only $\partial J_1/\partial \eta_p$ increases α, whereas $\partial J_2/\partial \eta_p$ keeps α unchanged. These results indicate that the distortion originates from a change in J_1, rather than a change in J_2, which is consistent with a previous study.[1]

In summary, we have explicitly studied the structural phase transition using NiO as an example. First, the energies of different types of magnetic order, types A and B, are found to degenerate in the cubic structure with both DFT calculations and MC simulations using a spin Hamiltonian model. However, type A is more stable in the distorted NiO structure. Further, we conclude that the spin–lattice coupling induces the rhombohedral contraction in NiO, according to symmetry analysis and DFT calculations. Therefore, the spin–lattice model is constructed to further understand the microscopic mechanism of the rhombohedral distortion with the strain item included. We apply both types A and B in our model, and the results show that the rhombohedral distortion only appears when the type-A magnetic structure is used, and it maintains the cubic symmetry when the type-B magnetic structure is considered. The results of DFT calculations are used as a comparison to ensure the accuracy of our model, and they show good consistency. Moreover, our model reveals that J_1 is responsible for the structural distortion, whereas the change in J_2 is irrelevant. Therefore, the mechanism of structural phase transition is demonstrated in this study, which also guides the understanding of similar phase transition phenomena in other monoxides.

Acknowledgments. The work at Fudan was sup-

ported by the National Natural Science Foundation of China (Grant Nos. 11825403, 12188101, and 11804138).

References

[1] Greenwald S and Smart J S 1950 *Nature* **166** 523
[2] Roth W L 1958 *Phys. Rev.* **110** 1333
[3] Schrön A, Rödl C and Bechstedt F 2012 *Phys. Rev. B* **86** 115134
[4] Sawatzky G A and Allen J W 1984 *Phys. Rev. Lett.* **53** 2339
[5] Rooksby H 1948 *Acta Crystallogr.* **1** 226
[6] Cracknell A P and Joshua S J 1969 *Mathematical Proceedings of the Cambridge Philosophical Society* **66** 493
[7] Sugiyama I, Shibata N, Wang Z, Kobayashi S, Yamamoto T and Ikuhara Y 2013 *Nat. Nanotechnol.* **8** 266
[8] Lin W, Chen K, Zhang S and Chien C L 2016 *Phys. Rev. Lett.* **116** 186601
[9] Machado F L A, Ribeiro P R T, Holanda J, Rodríguez-Suárez R L, Azevedo A and Rezende S M 2017 *Phys. Rev. B* **95** 104418
[10] Bartel L C and Morosin B 1971 *Phys. Rev. B* **3** 1039
[11] Toussaint C 1971 *J. Appl. Crystallogr.* **4** 293
[12] Krüger E 2020 *Symmetry* **12** 56
[13] Morosin B 1970 *Phys. Rev. B* **1** 236
[14] Cheetham A K and Hope D A O 1983 *Phys. Rev. B* **27** 6964
[15] Rodbell D S and Owen J 1964 *J. Appl. Phys.* **35** 1002
[16] Balagurov A M, Bobrikov I A, Sumnikov S V, Yushankhai V Y and Mironova-Ulmane N 2016 *JETP Lett.* **104** 88
[17] Li Y Y 1955 *Phys. Rev.* **100** 627
[18] Phillips T G and White R L 1967 *Phys. Rev.* **153** 616
[19] Pask J E, Singh D J, Mazin I I, Hellberg C S and Kortus J 2001 *Phys. Rev. B* **64** 024403
[20] Linnera J and Karttunen A J 2019 *Phys. Rev. B* **100** 144307
[21] Harrison W A 2007 *Phys. Rev. B* **76** 054417
[22] Kresse G and Furthmüller J 1996 *Comput. Mater. Sci.* **6** 15
[23] Kresse G and Joubert D 1999 *Phys. Rev. B* **59** 1758
[24] Perdew J P, Burke K and Ernzerhof M 1996 *Phys. Rev. Lett.* **77** 3865
[25] Dudarev S L, Botton G A, Savrasov S Y, Humphreys C J and Sutton A P 1998 *Phys. Rev. B* **57** 1505
[26] Li L and Kanai Y 2015 *Phys. Rev. B* **91** 235304
[27] Li X, Yu H, Lou F, Feng J, Whangbo M H and Xiang H 2021 *Molecules* **26** 26
[28] Lu X Z, Wu X and Xiang H J 2015 *Phys. Rev. B* **91** 100405
[29] Ni J Y, Li X Y, Amoroso D, He X, Feng J S, Kan E J, Picozzi S and Xiang H J 2021 *Phys. Rev. Lett.* **127** 247204
[30] Hutchings M T and Samuelsen E J 1972 *Phys. Rev. B* **6** 3447
[31] Shanker R and Singh R A 1973 *Phys. Rev. B* **7** 5000
[32] Coey J M D 2009 *Magnetism and Magnetic Materials* (New York: Cambridge University Press)
[33] Shull C G, Strauser W A and Wollan E O 1951 *Phys. Rev.* **83** 333
[34] Li J, Feng J, Wang P, Kan E and Xiang H 2021 *Sci. Chin. Phys. Mech. Astron.* **64** 286811